Journal of Alloys and Compounds 726 (2017) 1092–1100

Contents lists available at ScienceDirect

Journal of Alloys and Compounds

journal homepage: http://www.elsevier.com/locate/jalcom

Preparation of three-dimensional Ce-doped Sn_3O_4 hierarchical microsphere and its application on formaldehyde gas sensor

Xiaohui Ma [a], Jingli Shen [a], Dongxue Hu [a], Liang Sun [c], Yu Chen [a, c, **], Man Liu [b], Chuannan Li [a, ***], Shengping Ruan [a, b, *]

[a] State Key Laboratory on Integrated Optoelectronics, College of Electronic Science & Engineering, Jilin University, Changchun 130012, PR China
[b] State Key Laboratory on Applied Optics, Changchun 130023, PR China
[c] Global Energy Interconnection Research Institute, Beijing 102211, PR China

ARTICLE INFO

Article history:
Received 21 September 2016
Received in revised form
14 July 2017
Accepted 10 August 2017
Available online 12 August 2017

Keywords:
Sn_3O_4
Ce-doping
Hierarchical microspheres
Formaldehyde
Gas sensor

ABSTRACT

3-D hierarchical Sn_3O_4 and Ce-doped Sn_3O_4 microspheres assembled by nano-sheets were obtained by a one-step hydrothermal method and their formaldehyde sensing properties were investigated. The experiment results showed that the responses of the sensors based on Ce-Sn_3O_4 microspheres with different Ce-doping content were improved in different extents. The response of the optimal sensor based on Ce-Sn_3O_4 microspheres was 2.5 times higher than that of sensor based on Sn_3O_4 to 100 ppm formaldehyde. In addition, the sensors based on Ce-Sn_3O_4 microspheres showed good selectivity, repeatability, stability and fast response and recovery rate (about 4 s and 8 s to 200 ppm formaldehyde, respectively). Also, the possible mechanism of the improvement of formaldehyde sensing properties caused by Ce-doping was discussed.

1. Introduction

With the development of industry, environmental problems have become serious in recent years. Because toxic gases can cause damage to environment and human health, people pay great attention to detecting volatile organic compounds (VOC) including xylene, acetone and formaldehyde etc. [1] Among these VOC gases, the most concerned is formaldehyde due to its carcinogenicity according to the World Health Organization (WHO), and it is the main pollutant after home decoration. And formaldehyde has been considered as the main reason for sick building syndrome (SBS) [2]. Even in a low concentration, it would cause discomfort, such as headache, fatigue, difficult breathing and so on. Hence, the detection of formaldehyde is imperative, and the formaldehyde gas sensors with excellent properties are in demand. Various electrochemical [3,4], electrical, potentiometric [5], and piezoelectric sensors for the detection of formaldehyde have been developed during the past five decades. Semiconductor gas sensors have been increasingly attracting people's attention, owing to its portability, low cost, and convenient operation. To detect formaldehyde, various metal oxide materials, such as WO_3 [6], NiO [7], Co_3O_4 [8] and ZnO [9], have been used to fabricate gas sensors due to their good physical and chemical properties.

It is known that tin oxide is an important metal oxide, which has been widely applied in many fields, such as photocatalysis [10], lithium-ion battery [11], solar cell and gas sensor [12]. In the gas sensor field, SnO_2 have been widely researched, while other oxides with different valences of tin are seldom reported. SnO_2 and SnO are the most common form of tin oxide, and they could be used to compose many materials like Sn_2O_3, Sn_3O_4 and Sn_5O_6. All of these compounds contain oxidation states of +4 and + 2. Among them, Sn_3O_4, an n-type semiconductor with a band gap of 2.2 eV–2.9 eV [13], was first reported by Lawson in 1967 and showed a promising application prospect in many fields [14]. In recent years, Sn_3O_4 with various morphologies such as nano-belts and nano-flower [15] has been synthesized, and used as gas sensor. Sn_3O_4 nano-belts were successfully grown in a carbothermal evaporation process by

* Corresponding author. State Key Laboratory on Integrated Optoelectronics, College of Electronic Science & Engineering, Jilin University, Changchun 130012, PR China.
** Corresponding author. State Key Laboratory on Integrated Optoelectronics, College of Electronic Science & Engineering, Jilin University, Changchun 130012, PR China.
*** Corresponding author.
E-mail addresses: chenwy@jlu.edu.cn (Y. Chen), licn@jlu.edu.cn (C. Li), ruansp@jlu.edu.cn (S. Ruan).

http://dx.doi.org/10.1016/j.jallcom.2017.08.079
0925-8388/

Berengue etc. in 2010 [16]. Besides, Sn_3O_4 was synthesized via hydrothermal as a photocatalyst for water splitting by Manikandan etc. in 2014 [17]. In the field of gas sensor, it was usually used to detect ethanol [18]. However, formaldehyde sensor based on Sn_3O_4 was rarely reported.

In this paper, 3-dimensional pure Sn_3O_4 hierarchical microspheres and Ce-doped Sn_3O_4 hierarchical microspheres with different Ce content were successfully synthesized through a one-step hydrothermal method, and their micromorphology, crystal structure and element chemical state were characterized by XRD, SEM, TEM, and XPS. Then the influence on the formaldehyde sensing properties caused by Ce-introducing was investigated. The results indicated Ce-introducing efficiently improved formaldehyde sensing properties of Sn_3O_4 materials and the Ce-doped Sn_3O_4 sensor showed the enhanced sensitivity, fast response and recovery rate, good repeatability and stability. The possible mechanism on the improved gas sensing properties caused by Ce-doping was also discussed.

2. Experimental section

2.1. Chemical reagents

All the reagents are of analytical grade and used without any further treatment including: tin (II) dichloride dihydrate ($SnCl_2{\cdot}2H_2O$, Mw = 225.65), sodium hydroxide (NaOH, Mw = 40.00), sodium citrate dihydrate ($Na_3C_6H_5O_7{\cdot}2H_2O$, Mw = 294.10) and Cerium (III) nitrate hexahydrate ($Ce(NO_3)_3{\cdot}6H_2O$, Mw = 434.12), ethanol (C_2H_5OH, Mw = 46.07).

2.2. Preparation of Sn_3O_4 and Ce-Sn_3O_4 hierarchical microsphere

The synthesis of Sn_3O_4 and Ce-Sn_3O_4 was carried out by a one-step hydrothermal method. Firstly, ethanol and dissolved water were mixed with the volume ratio of 1:1 and then $SnCl_2{\cdot}2H_2O$ (0.9 g), NaOH (4 mmol), sodium citrate dihydrate (1 mmol) and different contents of $Ce(NO_3)_3{\cdot}6H_2O$ (the Ce/Sn atom ratio of 0, 3%, 6.67% and 9%) were added into above solution under constant stirring for 5 h. Then the solution was transferred into a 50 ml Teflon-lined stainless steel autoclave. The autoclave was heated at 180 °C for 10 h, and then cooled down to room temperature naturally. The precipitates were separated by centrifugation, washed with distilled water and ethanol for several times, and dried at 80 °C for 20 h. During the synthesis process of Sn_3O_4 hierarchical microsphere, the following reaction occurred:

$$4\ SnCl_2 + 2\ NaOH \rightarrow Sn_4(OH)_2Cl_6 + 2\ NaCl \quad (1)$$

$$Sn_4(OH)_2Cl_6 + 6\ NaOH \rightarrow 4\ SnO + 6\ NaCl + 4\ H_2O \quad (2)$$

$$6\ SnO + O_2 \rightarrow 2\ Sn_3O_4 \quad (3)$$

The as-prepared Ce-Sn_3O_4 samples with Ce/Sn atom ratio of 3%, 6.67% and 9% were denoted as 3% Ce-Sn_3O_4, 6.67% Ce-Sn_3O_4 and 9% Ce-Sn_3O_4 samples, respectively.

2.3. Characterization

The products were characterized by X-Ray diffraction (XRD, Shimadzu XRD-6000, Cu- Kα radiation λ = 1.5418 A); Scanning electron microscopy (SEM, SHIMADZU SSX-550); Transmission electron microscope (TEM, JEM-ARM200F). And X-Ray photoelectron spectroscopy (XPS) data was obtained with a VG ESCALAB MK II spectrometer with an Mg Kα excitation (1253.6 eV).

2.4. Fabrication and measurement of gas sensor

The details of the sensor fabrication were similar to our previous work [19]. To fabricate the gas sensor, the as-prepared materials were mixed with suitable water to form a paste. Then paste was coated on a ceramic tube. On the surface of the tube a pair of parallel Au electrodes was fabricated beforehand by jetting Au paste on ceramic tube through a metal-jetting system (MJ-10, Beijing Elite Tech Co., Ltd., China) and Pt wires were attached to the Au electrodes acting as conductive leads. Finally, a Ni-Cr heating wire, as a heater to control the operating temperature, was inserted into the tube and welded on a pedestal together with the Pt wires. The structure of the sensor was shown in Fig. 1. After the as-fabricated gas sensors aged at 200 °C for 72 h, their gas sensing properties were measured by CGS-8 intelligent gas sensing analysis system (Beijing Elite Tech Co., Ltd., China) under laboratory condition (25 °C, 40 RH%). The tested gas sample were prepared by injecting certain amount of target gas (CO, NO_2, NH_3 etc.) or volatile organic compounds (ethanol, acetone, formaldehyde, toluene etc.) into the test chamber (1 L in volume) full of air by a microsyringe. The response value (S) was defined as $S = R_a/R_g$, where R_a and R_g denoted the sensor's resistance in the air and presence of the target gases. The time taken by the sensor to achieve 90% of the total resistance change was defined as response time when the sensor exposed to the target gas (target gas adsorption) or the recovery time when the sensor went back to air ambience (target gas desorption).

3. Result and discussion

3.1. Structural and morphological characteristics

The XRD patterns of the as-prepared materials were shown in Fig. 2. For pure Sn_3O_4 hierarchical microspheres, it can be observed that all of the diffraction peaks can be indexed to the triclinic Sn_3O_4 from the Joint Committee on Powder Diffraction Standards card (JCPDS, 16-0737). In XRD pattern of Ce-Sn_3O_4 hierarchical microspheres, except for the diffraction peaks of Sn_3O_4, no obvious peak corresponding to Ce-contained compound can be found, which may be because Ce atoms entered Sn_3O_4 lattices and substituted Sn atoms. To investigate the thermostability of the as-prepared samples in crystal structure and composition, 6.67% Ce-Sn_3O_4 samples annealed under different temperature (from 100 °C to 300 °C) for 1 h were characterized by XRD, as shown in Fig. 2 (b). It can be observed that all the XRD patterns of the 6.67% Ce-Sn_3O_4 sample after annealing are same to that of the one without annealing indicating the as-prepared samples have a good thermostability under 300 °C.

To make sure chemical state of the elements, X-ray

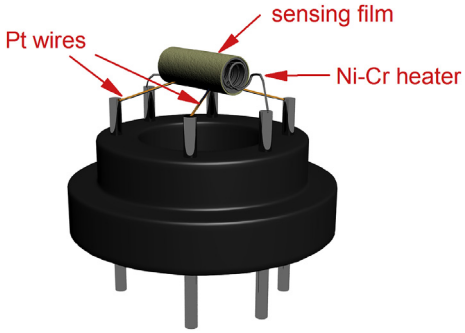

Fig. 1. Schematic structure of a completed gas sensor.

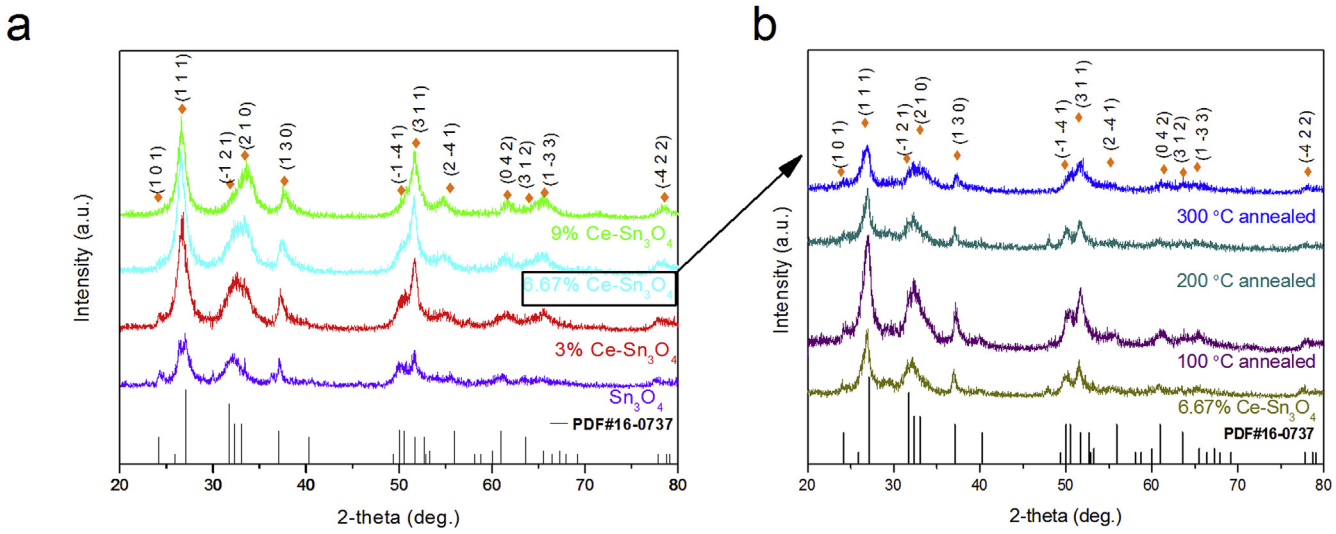

Fig. 2. XRD patterns of (a) as-prepared samples and (b) 6.67% Ce-Sn_3O_4 sample after being annealed at different temperature.

photoelectron spectroscopy (XPS) spectra of Ce-Sn_3O_4 with Ce/Sn atom ratio of 6.67% is investigated as shown in Fig. 3. Fig. 3(a) displays the XPS spectra survey of the sample. Fig. 3(b) shows the XPS spectra of Ce element and the existence of Ce-related peak can be observed demonstrating the existence of Ce element in the sample. According to the fitted peaks, the Ce element in the sample is present in both Ce^{4+} and Ce^{3+} oxidation states whose binding energies are 917.65 eV and 886.67 eV, respectively. Fig. 3(c) shows that the Sn 3d doublet characterized by $3d_{3/2}$–$3d_{5/2}$ splitting peak is observed clearly. The Sn $3d_{5/2}$ spectra of Sn_3O_4 could be dissolved into two peaks, the peak at 487.3 eV is ascribed to Sn^{4+}, while the peak at 486.3 eV is attributed to Sn^{2+}. This reflects the different kinds of chemical environment for the Sn element in the Sn_3O_4. Also the Sn $3d_{3/2}$ spectra can be dissolved into two peaks at 497.2 eV and 493.3 eV, which are assigned to Sn^{2+} and Sn^{4+}, respectively. From Fig. 3(d) we could found that O_{1s} signal is

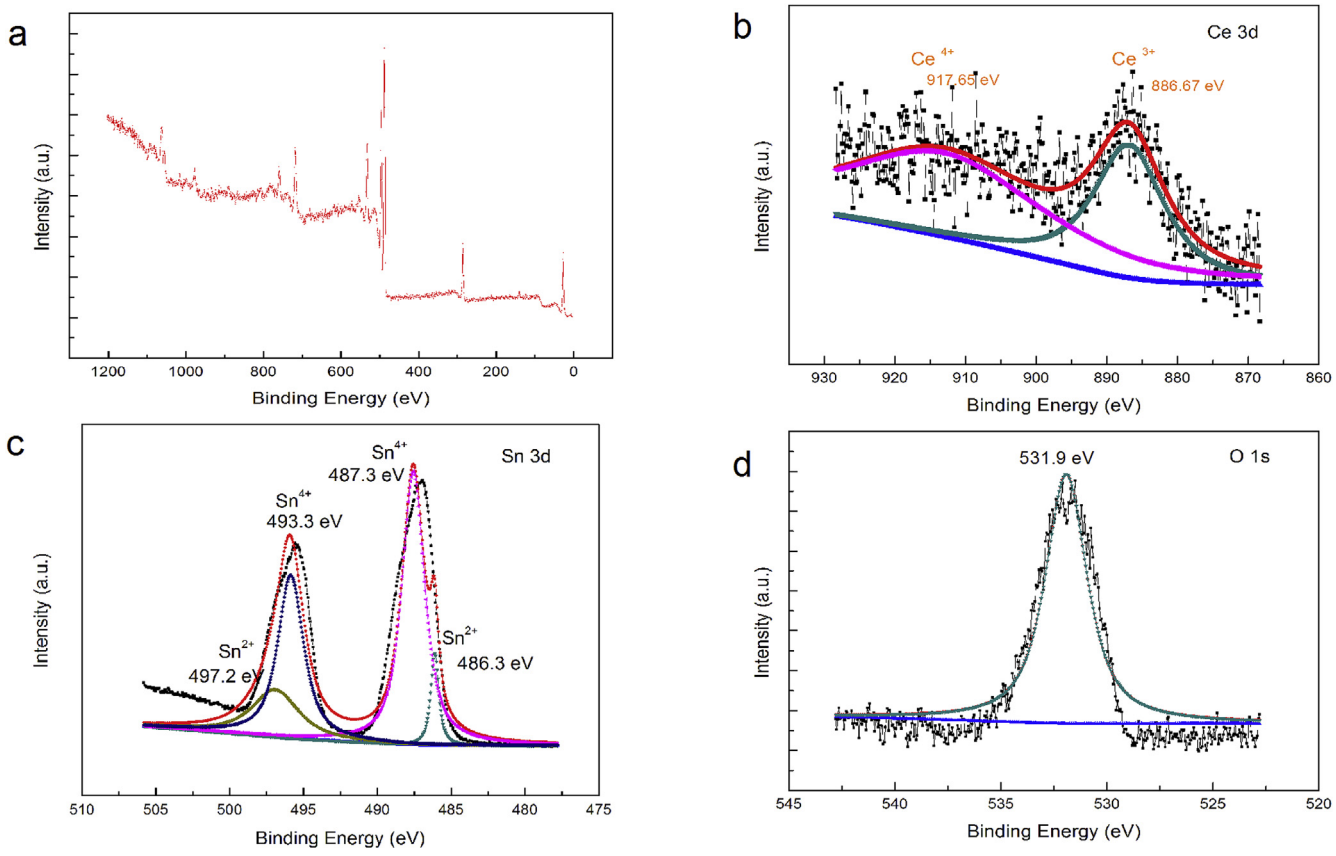

Fig. 3. XPS spectra of the Ce-Sn_3O_4 hierarchical microspheres with Ce/Sn atom ratio of 6.67%: (a) survey, (b) Ce element, (c) Sn element and (d) O element.

symmetric indicating that one kind of oxygen specie is present on the surface of the sample. The peak centered at 531.9 eV is ascribed to O^{2-}.

The morphologies of the as-prepared Sn_3O_4 and Ce-Sn_3O_4 samples are characterized by SEM, as shown in Fig. 4(a)-(g). It could be found from the low magnification SEM images in Fig. 4(a)-(d), both of Sn_3O_4 and Ce-Sn_3O_4 samples show the flower-like microspheres with a diameter of 2.5–6 μm indicating the Ce-introducing doesn't make obvious effects on the micromorphology and size distribution. In the inserts of Fig. 4(a)-(d), the high magnification SEM images show that the 3-D hierarchical nanostructures of Sn_3O_4 and Ce-Sn_3O_4 are consist of thin sheets with an average thickness of 25 nm. Fig. 4 (e)-(g) presents the morphologies of sample of 6.67% Ce-Sn_3O_4 sample annealed at 100 °C, 200 °C and 300 °C for 1 h, respectively. It can be observed that annealing process doesn't make obvious effects on the micromorphology including size and surface roughness.

To further characterize the microscopic morphology and structure of Ce-Sn_3O_4 hierarchical microspheres, TEM and HRTEM were carried out as shown in Fig. 5. Fig. 5(a) shows the low-resolution TEM of an individual Ce-Sn_3O_4 hierarchical microsphere with a diameter of 2.5 μm, which is composed of nanosheets, and a typical thickness of the nanosheet is 23 nm. Fig. 5(b) shows high resolution TEM image of a nanosheet. The measured interplanar distances of 0.328 nm and 0.242 nm are consistent with (1 1 1) and (1 3 0) d-spacing of Sn_3O_4, respectively.

3.2. Gas sensor performance

The gas sensing properties of the as-prepared Sn_3O_4 and Ce-Sn_3O_4 hierarchical microspheres for formaldehyde including optimum operating temperature, selectivity, response-recovery time, repeatability and stability were investigated.

The response of a gas sensor based on semiconductor material is intensively affected by the operating temperature. To determine the optimum operating temperature, the responses of the sensors based on Sn_3O_4 and Ce-Sn_3O_4 hierarchical microspheres to 100 ppm formaldehyde were tested at the operating temperature from 65 to 325 °C, as shown in Fig. 6. It could be found that the response values of all the sensors increased with the raise of operating temperature until they reached their maximum at 200 °C and then decreased with the further increase of operating temperature. Therefore, 200 °C was regarded as the optimal operating temperature. The sensor based on Ce-Sn_3O_4 hierarchical microspheres with Ce/Sn atom ratio of 6.67% showed the highest response of 5.5 among all the sensors at 200 °C, which was 2.5 times as high as that of the sensor based on pure Sn_3O_4 hierarchical microspheres. In addition, compared with that of the Sn_3O_4 hierarchical microspheres, all the sensors based on the as-prepared Ce-Sn_3O_4 samples showed enhanced responses, indicating that Ce-doping can improve the response of Sn_3O_4 to formaldehyde.

Selectivity is another important property, which shows the ability to distinguish different gases. To understand the selectivity, the response of the sensor based on Ce-Sn_3O_4 was tested for

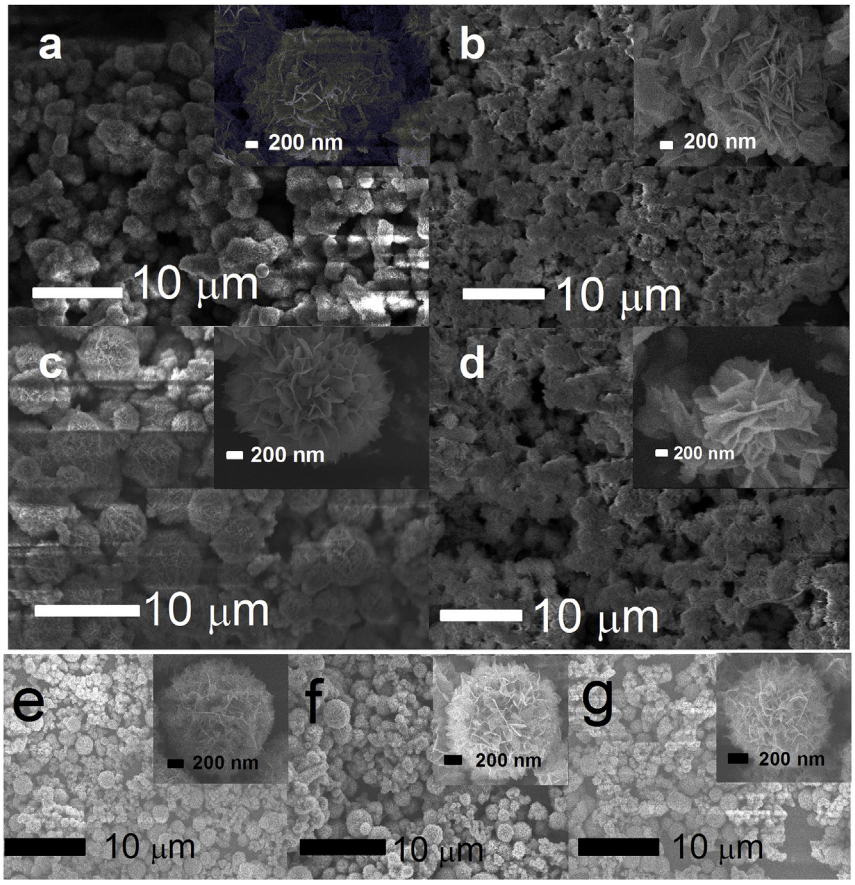

Fig. 4. SEM images of the as-prepared (a) pure Sn_3O_4, (b) 6.67% Ce-Sn_3O_4, (c) 6.67% Ce-Sn_3O_4, (d) 6.67% Ce-Sn_3O_4 sample, and (e)–(g) 6.67% Ce-Sn_3O_4 sample after being annealed at different temperature; the insets are the corresponding high magnification SEM images.

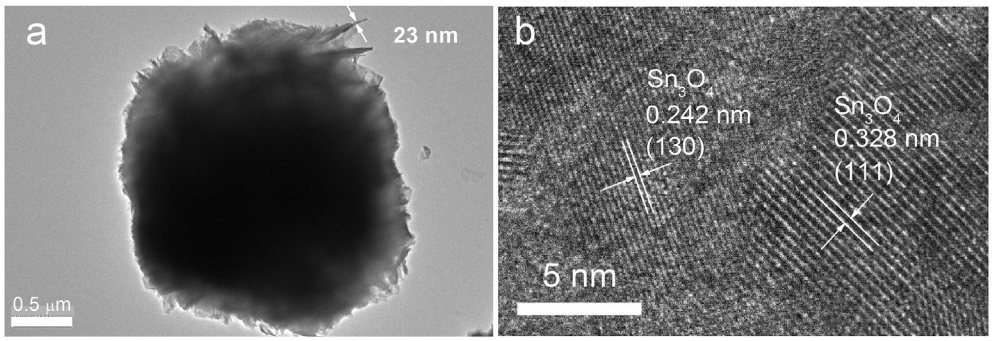

Fig. 5. (a) Low-resolution and (b) high-resolution TEM images of the as-prepared Ce-Sn_3O_4 hierarchical microspheres with Ce/Sn atom ratio of 6.67%.

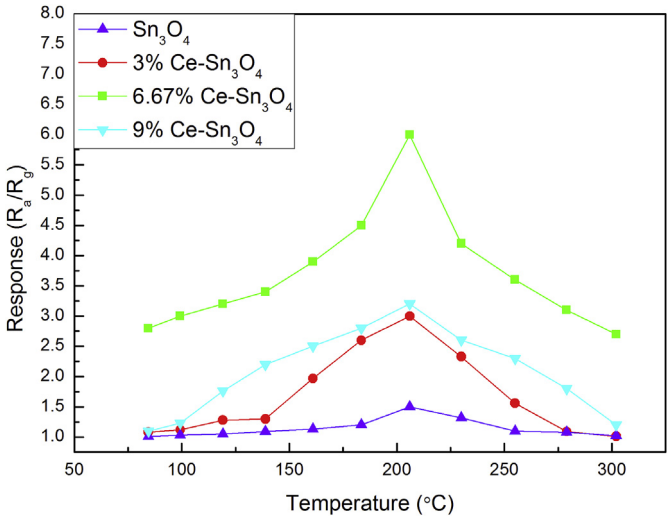

Fig. 6. Response of sensors based on Sn_3O_4 and Ce-Sn_3O_4 hierarchical microspheres to 100 ppm formaldehyde at different operating temperature.

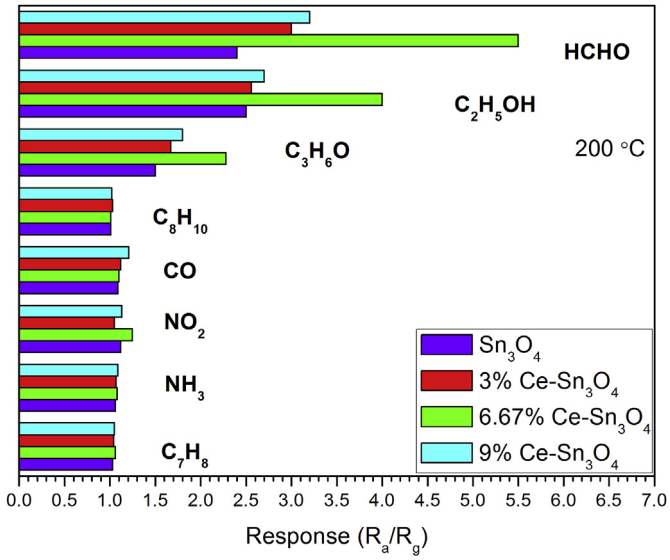

Fig. 7. Selectivity of the sensor based on pure Sn_3O_4 and Ce-Sn_3O_4 hierarchical microspheres to 100 ppm HCHO, C_2H_5OH, C_3H_6O, C_8H_8, CO, NO_2, NH_3, and C_7H_8 at 200 °C.

100 ppm different kinds of gases. Fig. 7 showed the response of the sensors based on the Sn_3O_4 and Ce-Sn_3O_4 hierarchical microspheres to 100 ppm formaldehyde (HCHO), ethanol (C_2H_5OH), acetone (C_3H_6O), xylene (C_8H_8), carbon monoxide (CO), nitrogen dioxide (NO_2), ammonia (NH_3), and toluene (C_7H_8) at the optimum operating temperature. The sensor based on Sn_3O_4 hierarchical microspheres showed a higher response value to formaldehyde than those to other gases, but a little lower than that to ethanol indicating its poor selectivity to formaldehyde. For Ce-Sn_3O_4 hierarchical microspheres based sensors, especially the 6.67% Ce-Sn_3O_4 based one, they showed good sensitivity to formaldehyde among the target gases and the selectivity between formaldehyde and ethanol was improved due to the Ce-doping.

Fig. 8 shows the response of sensors based on Sn_3O_4 and Ce-Sn_3O_4 hierarchical microspheres versus the formaldehyde concentration ranging from 1 to 300 ppm at 200 °C. According to the experimental result, the responses of the Ce-Sn_3O_4 based sensor raised rapidly with the increase of formaldehyde concentration, while the Sn_3O_4 based sensor presented a lower response. Also, it is clear that the sensor based on Ce-Sn_3O_4 hierarchical microspheres with Ce/Sn atom ratio of 6.67% showed highest response among all the samples.

Response and recovery time is an important parameter and fast response-recovery rate is good to real-time detection for a practical gas sensor. Fig. 9(a) showed the response-recovery curves of the four sensors to different concentration of formaldehyde at the optimum operating temperature. When the sensors underwent formaldehyde gas, the resistance decreased rapidly, and when the

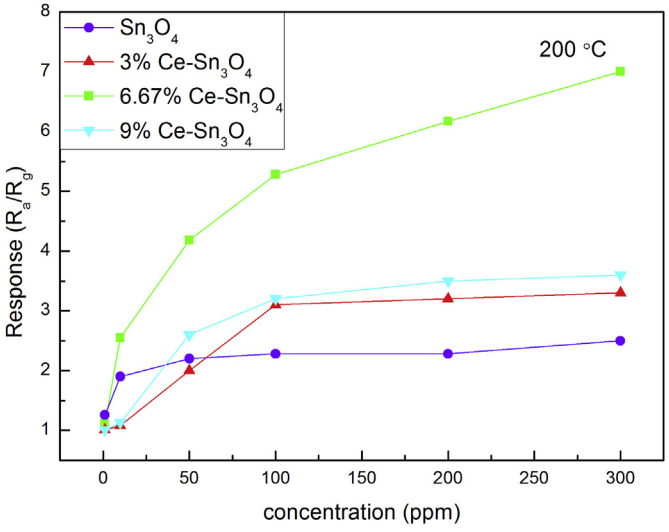

Fig. 8. Curves of responses of the sensors based on pure Sn_3O_4 and Ce-Sn_3O_4 hierarchical microspheres versus formaldehyde concentration at 200 °C.

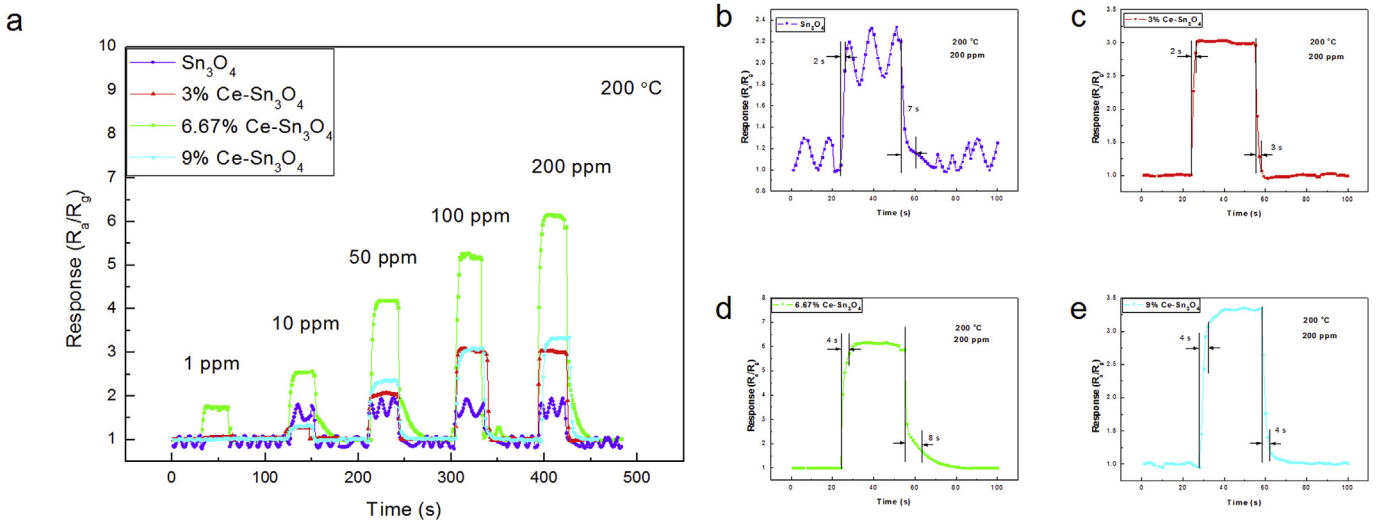

Fig. 9. Transient response curves of the pure Sn_3O_4 and Ce-Sn_3O_4 hierarchical microspheres based sensors to (a) 1–200 ppm and (b)–(e) 200 ppm formaldehyde at 200 °C.

sensor exposed to air, the resistance recovered also rapidly. From Fig. 9(b)-(e) as we can see, to 200 ppm formaldehyde, the response time of the four sensors were 2 s, 2 s, 4 s and 4 s and the recovery time of the four sensors were 7 s, 3 s, 8 s and 4 s respectively. A comparison between some reported formaldehyde sensors and Ce-Sn_3O_4 based sensors was provided in Table 1 [20–24]. And it can be found the 6.67% Ce-Sn_3O_4 based sensors have advantages on operating temperature, sensitivity, and response/recovery time for formaldehyde detection.

A long-term stability of the Sn_3O_4 and Ce-Sn_3O_4 based sensors to 100 ppm formaldehyde within 40 days were showed in Fig. 10(a). Responses of all the sensors gradually decreased and became relatively stable. For Ce-Sn_3O_4 based sensors, especially the one with Ce/Sn atom ratio of 6.67%, the change in response values was small and sensor could keep high sensitivity to formaldehyde within 40 days indicating their good stability. The repeatability of sensors based on pure Sn_3O_4 and Ce-Sn_3O_4 to 100 ppm formaldehyde was tested consecutively. The results were shown in Fig. 10(b)-(e). During the test, the resistance of the pure Sn_3O_4 and Ce-Sn_3O_4 based sensors in air was almost unchanged and so did in formaldehyde ambience, i.e. the response values were stable. Also, the response and recovery time unchanged for each sensor. These indicated the pure Sn_3O_4 and Ce-Sn_3O_4 based sensors have good repeatability.

3.3. Gas sensing mechanism

The gas sensing mechanism of Sn_3O_4 hierarchical microspheres based sensor, illustrating in Figs. 11 and 12, can be explained through space electronic transfer model. The process involves adsorption of gas, electronic transfer and desorption of gas. When Sn_3O_4 hierarchical microspheres are exposed to air, oxygen molecules will adsorb on their surface and form ionized oxygen species (O^{2-}, O^- and O_2^-, and O^- is the dominated at 200 °C) by capturing electrons from the conduction band of Sn_3O_4, which will lead to an increase in sensor's resistance [25–28]. When the sensor undergoes the reducing formaldehyde, formaldehyde molecules will react with the chemisorbed oxygen-ions and the captured electrons return back to the conduction band of Sn_3O_4, leading to a decrease in sensor's resistance. When the sensor is exposes to air again, chemisorbed oxygen-ions will absorb and the sensor will recover to its original state. The related equations are shown as follows:

$$O_{2\ (gas)} \rightarrow O_{2\ (ads)} \quad (4)$$

$$O_{2\ (ads)} \rightarrow O^{2-}{}_{(ads)} \quad (5)$$

$$O_{2\ (ads)} \rightarrow O^{-}{}_{(ads)} \quad (6)$$

Table 1
Comparison of various formaldehyde gas sensors.

Material	Synthesis method	Optimum operating temperature	Response/recovery time (s)	Response	Reference
Cd-Doped TiO_2-SnO_2	sol-gel	593 K	20/17	3 (200 ppm)	[20]
In_2O_3Nanofibers	electro-spinning	340 °C	18/17	3.113 (100 ppm)	[21]
In_2O_3Nanoribbons	electro-spinning	300 °C	16/15	4.214 (100 ppm)	[21]
$La_{0.68}Pb_{0.32}FeO_3$ nanomaterials	sol-gel	180 °C	25/20	4.5 (100 ppm)	[22]
TiO_2–Ag nanocomposite	sol–gel	360 °C	30/45	3.25 (200 ppm)	[23]
ZnO+5%MnO_2	screen-printing technology and solution growth process	320 °C	39/24	23 (200 ppm)	[24]
6.67% Ce-Sn_3O_4	hydrothermal	200 °C	4/8	5.5 (100 ppm)	This work

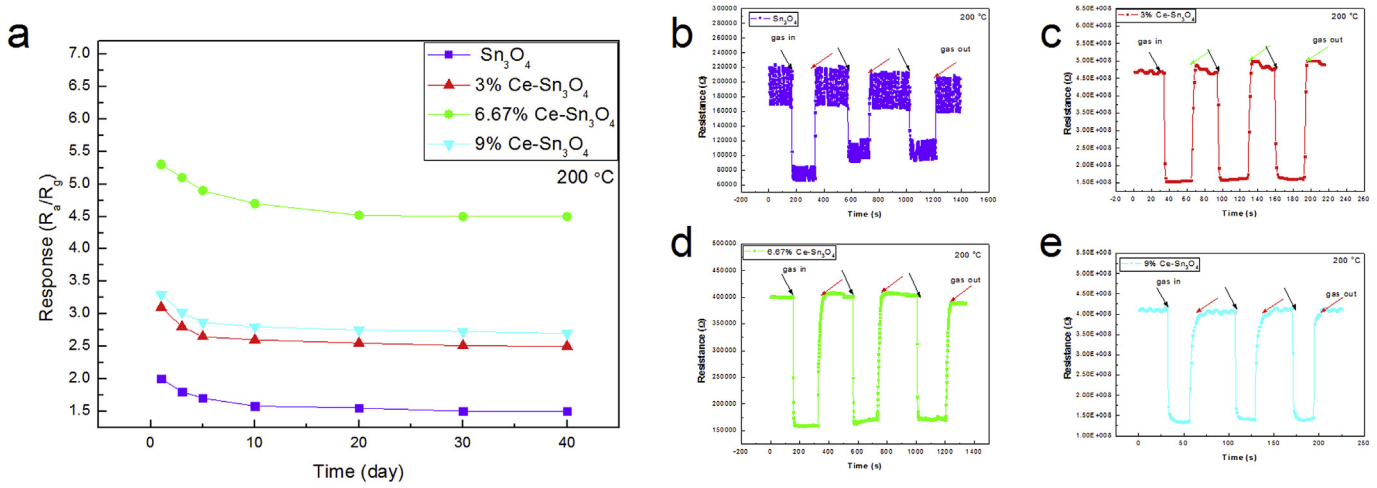

Fig. 10. (a) Stability and (b–e) repeatability of the pure Sn_3O_4 and Ce-Sn_3O_4 hierarchical microspheres based sensors at 200 °C.

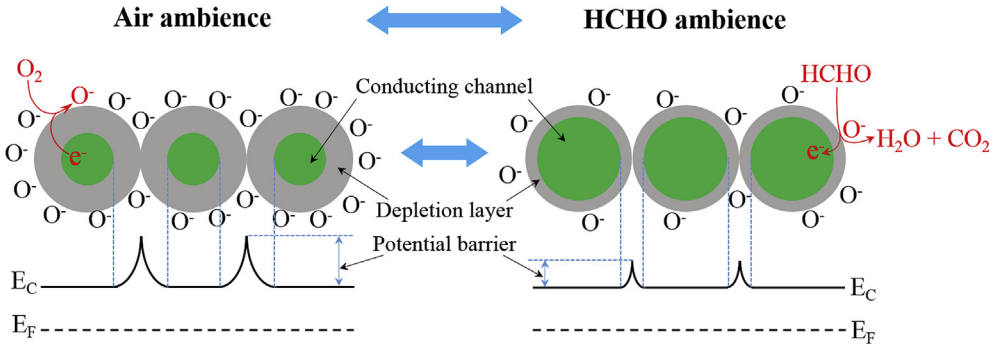

Fig. 11. A sketch of HCHO sensing mechanism of Sn_3O_4 and Ce-Sn_3O_4 samples.

$$O_{2\,(ads)} + 2\,e^- \rightarrow O_{2\,(ads)}^- \quad (7)$$

$$HCHO_{\,(gas)} + 2\,O^-_{\,(ads)} \rightarrow CO_{2\,(gas)} + H_2O_{\,(gas)} + 2\,e^- \quad (8)$$

Besides, the improved sensitivity to formaldehyde is probably attributed to the catalytic oxidation of element Ce to formaldehyde [29]. The illustration of the mechanism of enhanced formaldehyde (HCHO) sensing properties of Ce-Sn_3O_4 induced by the catalysis of Ce doping is showed in Fig. 12(b). The redox Ce^{4+}-Ce^{3+} couple has the ability to change from Ce^{4+} under oxidizing conditions to Ce^{3+} under reducing conditions and vice versa [30] In air ambience, the majority of Ce atoms are in the form of Ce^{4+}. When Ce-Sn_3O_4 expose to HCHO ambience, some HCHO molecules will adsorb on the surface lattice oxygen anion or chemisorb oxygen species next to Ce^{4+} and form the HO-CHO surface species. Then HO-CHO species desorb from the surface of Ce-Sn_3O_4 by further oxidizing into H_2O and CO_2 while Ce^{4+} are reduced to Ce^{3+}. Thus the HCHO sensing process shown as equation (8) is promoted and the response of the sensor based on Ce-Sn_3O_4 is enhanced. When the Ce-Sn_3O_4 is exposed to air ambience again, Ce^{3+} will transform back into Ce^{4+}. The existence of redox Ce^{4+}-Ce^{3+} couple makes the sensor show a higher resistance in air ambience by broadening the depletion region in Ce-Sn_3O_4 hierarchical microspheres (narrowing the conducting channel) and increasing the potential barrier between Ce-Sn_3O_4 nanocrystallines. And the catalysis of redox Ce^{4+}-Ce^{3+} couple makes the sensor show a lower resistance in HCHO ambience by broadening the depletion region in Ce-Sn_3O_4 nanocrystallines and decrease the height of the potential barrier between Ce-Sn_3O_4 nanocrystallines. So, compared with pure Sn_3O_4, Ce-Sn_3O_4 based sensor shows a larger resistance change, i.e. a higher response during HCHO sensing process.

The reason that the sensor based on 6.67% Ce-Sn_3O_4 hierarchical microspheres showed better sensing properties has been discussed. The gas sensing response value increased gradually with the increase of Ce-doping atomic percentage from 3% to 6.67%, but decreased gradually when the doping percentage was higher than 6.67%. On the hand, redox Ce^{3+}-Ce^{4+} couple in Ce-Sn_3O_4 hierarchical microspheres can effectively promote the HCHO sensing reactions and thus the sensitivity of Ce-Sn_3O_4 hierarchical microspheres to HCHO will improve with the increase in Ce-doping percentage when it is relatively low. However, on the other hand, Ce atoms enter Sn_3O_4 lattices and substitute Sn atoms will break the long-range order of Sn_3O_4. As a result, the scatter of charged carriers in Ce-Sn_3O_4 hierarchical microspheres during the transport will gradually enhance with the increase in Ce-doping percentage and affect the resistance of the Ce-Sn_3O_4 based sensor. When Ce-doping percentage is high enough, the catalysis of Ce^{3+}/Ce^{4+} redox couple for HCHO sensing reactions will be restricted due to the limited surface of Ce-Sn_3O_4. The redundant surface and internal Ce atoms in Ce-Sn_3O_4 will scatter the electrons released from chemisorbed oxygen species instead of promoting the HCHO sensing reactions and thus the change in resistance, i.e. the response of Ce-Sn_3O_4 based sensor to HCHO will decrease with the further increase of Ce percentage when it is higher than the optimal value.

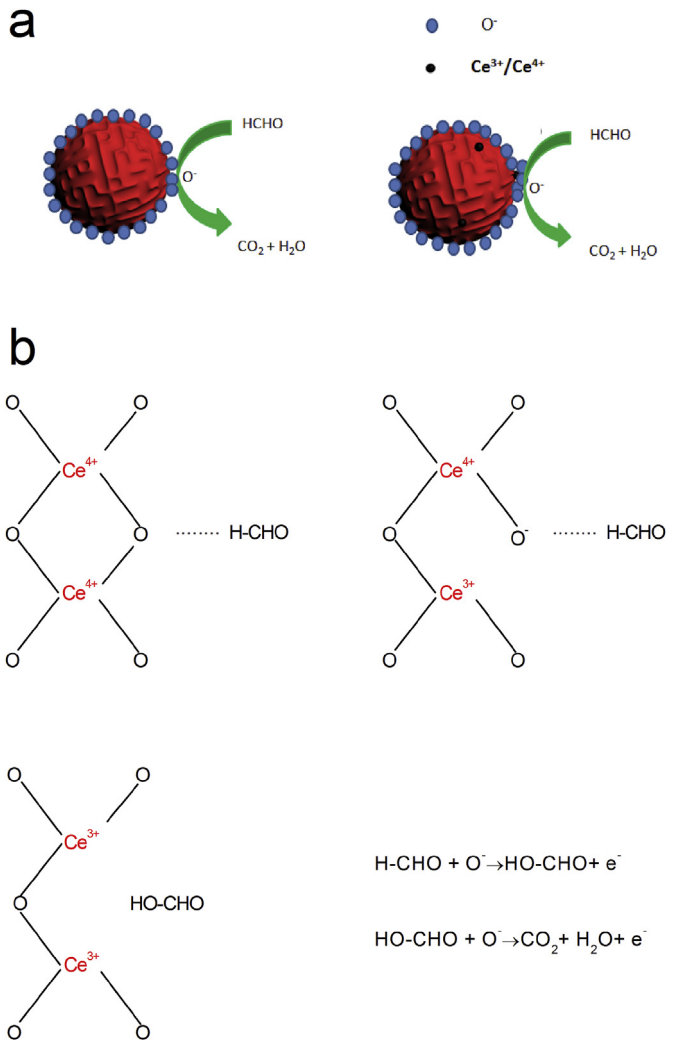

Fig. 12. The illustration of formaldehyde sensing mechanism: (a) reaction occurred on the surface of Sn_3O_4 and Ce-Sn_3O_4 hierarchical microspheres, (b) reaction between formaldehyde and Ce^{4+}-Ce^{3+} couple in Ce-Sn_3O_4 hierarchical microspheres.

4. Conclusions

In summary, we successfully synthesized 3-D Sn_3O_4 hierarchical microspheres and Ce-Sn_3O_4 hierarchical microspheres with different Ce content by a simple one-step hydrothermal method. Analysis by XPS confirmed the presence of Ce^{3+} and Ce^{4+} in the resultant material. The SEM and TEM characterization indicated that the Sn_3O_4 microsphere had an average size of about 3 μm and is composed by single crystalline Sn_3O_4 nanosheets. The sensors based on Ce-Sn_3O_4, especially the one with Ce/Sn atom ratio of 6.67%, exhibited enhanced sensing properties to formaldehyde compared with pure Sn_3O_4 at 200 °C. It is convinced that Ce^{3+} and Ce^{4+} serve particular function of catalyzing formaldehyde oxidation and improving the sensitivity of Ce-Sn_3O_4 hierarchical microspheres to formaldehyde.

Acknowledgements

The authors are grateful to National Natural Science Foundation of China (Grant No. 11574110, 61404058), Project of Science and Technology Development Plan of Jilin Province (20160204013GX), Postdoctoral Science Foundation of China (Grant No. 2016M600231), Opened Fund of the State Key Laboratory on Integrated Optoelectronics, Opened Fund of the State Key Laboratory on Applied Optics, and State Grid Corporation of China (SGRIDGKJ [2015]959).

References

[1] G. Wieslander, D. Norbäck, E. Björnsson, C. Janson, G. Boman, Asthma and the indoor environment: the significance of emission of formaldehyde and volatile organic compounds from newly painted indoor surfaces, Int. Arch. Occup. Environ. Health 69 (1996) 115–124.
[2] S. Li, F. Li, Z. Rao, A novel and sensitive formaldehyde gas sensor utilizing thermal desorption coupled with cataluminescence, Sens. Actuators B Chem. 145 (2010) 78–83.
[3] M. Hämmerle, E.A. Hall, N. Cade, D. Hodgins, Electrochemical enzyme sensor for formaldehyde operating in the gas phase, Biosens. Bioelectron. 11 (1996) 239–246.
[4] Y. Herschkovitz, I. Eshkenazi, C. Campbell, J. Rishpon, An electrochemical biosensor for formaldehyde, J. Electroanal. Chem. 491 (2000) 182–187.
[5] F. Vianello, A. Stefani, M. Di Paolo, A. Rigo, A. Lui, B. Margesin, M. Zen, M. Scarpa, G. Soncini, Potentiometric detection of formaldehyde in air by an aldehyde dehydrogenase FET, Sens. Actuators B Chem. 37 (1996) 49–54.
[6] L. Deng, X. Ding, D. Zeng, S. Tian, H. Li, C. Xie, Visible-light activate mesoporous WO_3 sensors with enhanced formaldehyde-sensing property at room temperature, Sens. Actuators B Chem. 163 (2012) 260–266.
[7] J.A. Dirksen, K. Duval, T.A. Ring, NiO thin-film formaldehyde gas sensor, Sens. Actuators B Chem. 80 (2001) 106–115.
[8] C. Ma, D. Wang, W. Xue, B. Dou, H. Wang, Z. Hao, Investigation of formaldehyde oxidation over Co_3O_4– CeO_2 and Au/Co_3O_4– CeO_2 catalysts at room temperature: effective removal and determination of reaction mechanism, Environ. Sci. Technol. 45 (2011) 3628–3634.
[9] X. Chu, T. Chen, W. Zhang, B. Zheng, H. Shui, Investigation on formaldehyde gas sensor with ZnO thick film prepared through microwave heating method, Sens. Actuators B Chem. 142 (2009) 49–54.
[10] M. Manikandan, T. Tanabe, P. Li, S. Ueda, G.V. Ramesh, R. Kodiyath, J. Wang, T. Hara, A. Dakshanamoorthy, S. Ishihara, K. Ariga, J. Ye, N. Umezawa, H. Abe, Photocatalytic water splitting under visible light by mixed-valence Sn(3)O(4), ACS Appl. Mater. Interfaces 6 (2014) 3790–3793.
[11] P. Gurunathan, P.M. Ette, K. Ramesha, Synthesis of hierarchically porous SnO_2 microspheres and performance evaluation as Li-Ion battery anode by using different binders, ACS Appl. Mater. interfaces 6 (2014) 16556–16564.
[12] H. Wang, K. Dou, W.Y. Teoh, Y. Zhan, T.F. Hung, F. Zhang, J. Xu, R. Zhang, A.L. Rogach, Engineering of facets, band structure, and gas-sensing properties of hierarchical Sn^{2+}-Doped SnO_2 nanostructures, Adv. Funct. Mater. 23 (2013) 4847–4853.
[13] P. Suman, E. Longo, J. Varela, M. Orlandi, Controlled synthesis of layered Sn_3O_4 nanobelts by carbothermal reduction method and their gas sensor properties, J. Nanosci. Nanotechnol. 14 (2014) 6662–6668.
[14] M.S. Wrighton, D.L. Morse, A.B. Ellis, D.S. Ginley, H.B. Abrahamson, Photoassisted electrolysis of water by ultraviolet irradiation of an antimony doped stannic oxide electrode, J. Am. Chem. Soc. 98 (1976) 44–48.
[15] W. Xu, M. Li, X. Chen, J. Zhao, R. Tan, R. Li, J. Li, W. Song, Synthesis of hierarchical Sn_3O_4 microflowers self-assembled by nanosheets, Mater. Lett. 120 (2014) 140–142.
[16] O. Berengue, R. Simon, A. Chiquito, C. Dalmaschio, E. Leite, H. Guerreiro, F.E.G. Guimarães, Semiconducting Sn_3O_4 nanobelts: growth and electronic structure, J. Appl. Phys. 107 (2010) 033717.
[17] M. Manikandan, T. Tanabe, P. Li, S. Ueda, G.V. Ramesh, R. Kodiyath, J. Wang, T. Hara, A. Dakshanamoorthy, S. Ishihara, Photocatalytic water splitting under visible light by mixed-valence Sn_3O_4, ACS Appl. Mater. Interfaces 6 (2014) 3790–3793.
[18] J. Liu, C. Wang, Q. Yang, Y. Gao, X. Zhou, X. Liang, P. Sun, G. Lu, Hydrothermal synthesis and gas-sensing properties of flower-like Sn_3O_4, Sens. Actuators B Chem. 224 (2016) 128–133.
[19] D. Jiang, W. Wei, F. Li, Y. Li, C. Liu, D. Sun, C. Feng, S. Ruan, Xylene gas sensor based on α-MoO_3/α-Fe_2O_3 heterostructure with high response and low operating temperature, RSC Adv. 5 (2015) 39442–39448.
[20] W. Zeng, T. Liu, Z.C. Wang, S. Tsukimoto, M. Saito, Y. Ikuhara, Selective detection of formaldehyde gas using a Cd-doped TiO_2-SnO_2 sensor, Sensors 9 (11) (2009) 9029–9038.
[21] Z. Li, Y. Fan, J. Zhan, In_2O_3 nanofibers and nanoribbons: preparation by electrospinning and their formaldehyde gas-sensing properties, Eur. J. Inorg. Chem. 2010 (21) (2010) 3348–3353.
[22] L. Zhang, J.F. Hu, P. Song, H.W. Qin, X.D. Liu, M.H. Jiang, Formaldehyde-sensing characteristics of perovskite $La_{0.68}$ $Pb_{0.32}$ FeO_3 nano-materials, Phys. B Condens. Matter 370 (1) (2005) 259–263.
[23] Z. Wen, L. Tian-Mo, L. De-Jun, Formaldehyde gas sensing property and mechanism of TiO_2–Ag nanocomposite, Phys. B Condens. Matter 405 (19) (2010) 4235–4239.
[24] C.S. Xie, L.Q. Xiao, M.L. Hu, Z.K. Bai, X.P. Xia, D.W. Zeng, Fabrication and formaldehyde gas-sensing property of ZnO–MnO_2 coplanar gas sensor arrays, Sens. Actuators B Chem. 145 (1) (2010) 457–463.
[25] N. Yamazoe, G. Sakai, K. Shimanoe, Oxide semiconductor gas sensors, Catal.

Surv. Asia 7 (2003) 63–75.
[26] D. Wang, S. Du, X. Zhou, B. Wang, J. Ma, P. Sun, Y. Sun, G. Lu, Template-free synthesis and gas sensing properties of hierarchical hollow ZnO microspheres, CrystEngComm 15 (2013) 7438–7442.
[27] N. Yamazoe, New approaches for improving semiconductor gas sensors, Sens. Actuators B Chem. 5 (1991) 7–19.
[28] M. Egashira, Y. Shimizu, Y. Takao, S. Sako, Variations in I–V characteristics of oxide semiconductors induced by oxidizing gases, Sens. Actuators B Chem. 35 (1996) 62–67.
[29] Y. Shen, X. Yang, Y. Wang, Y. Zhang, H. Zhu, L. Gao, M. Jia, The states of gold species in CeO_2 supported gold catalyst for formaldehyde oxidation, Appl. Catal. B Environ. 79 (2008) 142–148.
[30] C. Li, K. Domen, K. Maruya, T. Onishi, Dioxygen adsorption on well-outgassed and partially reduced cerium oxide studied by FT-IR, J. Am. Chem. Soc. 111 (20) (1989) 7683–7687.